

Role- of physical processes in regulating the biological responses in the Eastern Arabian Sea during the late southwest monsoon

¹K. Nandakumar, ¹Suhas S. Shetye, ¹Siby Kurian, ¹S. G. Aparna, ¹Mangesh Gauns, ²Shrikant Dora

¹CSIR-National Institute of Oceanography, Dona Paula-403 004, Goa, India

²Indian National Centre for Ocean Information Services, Ministry of Earth Sciences, Government of India, Hyderabad-500090, India

Abstract

Understanding physical properties and associated biological responses in the marine ecosystem is critical for fisheries and assessing the ocean's role in determining the fate of anthropogenic carbon dioxide emissions. This study reports the different roles of southwest monsoon (SWM) upwelling, oceanic fronts, and mesoscale eddies in supplying nutrients and fueling phytoplankton production in the eastern Arabian Sea (EAS). In-situ measurements of physical parameters along with the distribution of biogeochemical parameters in the 100m water column over a wide latitudinal transect from 8⁰N to 21⁰N (Station II-1 to II-14 at 1⁰ intervals) along the 68⁰E were carried out during the late SWM (September 11-19) of 2017 . We found distinct features in the study area from the in-situ measurements and satellite data. Primarily, oceanic fronts along with higher instabilities caused vertical mixing at stations II-6, and II-10 (13⁰N and 17⁰N). Secondly, eddy-induced lateral advection of high productive water from the Western Arabian Sea (WAS) resulted in high phytoplankton biomass at stations II-7, and II-8 (14⁰N,15⁰N), which led to high concentrations of pigments (chlorophyll-a (Chl-a), fucoxanthin). SWM upwelling induced higher phytoplankton biomass at northern stations II-13 and II-14 and is evident from the higher total organic carbon (TOC), high total bacterial count (TBC) and Chl-a concentration (up to 0.371 µg/L at II-14). The difference in time lag for vertical mixing in the station II-6 and II-10 are responsible for the contrasting biological responses in these stations. . The present study showed that along with SWM upwelling, eddy-induced lateral advection from WAS and oceanic fronts are also increasing phytoplankton biomass in the EAS. The present study suggests that the high phytoplankton biomass production prompted by upwelling, oceanic fronts, and mesoscale eddies can influence CO₂ sequestration and the prevailing subsurface oxygen minimum zone in the EAS.

Keywords: Mesoscale eddies, Oceanic fronts, Upwelling, Arabian Sea, Chlorophyll a

Introduction

Arabian Sea (AS) is a semi-enclosed dynamic oceanic basin in the northern Indian Ocean, well known for its high productivity and oxygen minimum zone (OMZ) (Wyrki, 1971, Naqvi, 1987; Pfannkuche and Lochte, 2000; Prasanna Kumar et al., 2001). The semi-annual reversal of monsoonal winds makes the biogeochemical features of the AS unique among world oceans. These reversing monsoon winds enhance the biological productivity in the AS through distinct mechanisms. Strong upwelling enhances the productivity in the continental shelf of Somalia, Arabia, and the southwest coast of India during southwest monsoon (SWM) (Bauer et al., 1991; Brock et al., 1991; Smith et al., 1998), whereas convective mixing builds up productivity in the north and the central AS during the northeast monsoon (NEM) (Madhupratap et al., 1996; Wiggert et al., 2002; Prasanna Kumar et al., 2009). In addition to these monsoon winds, mesoscale features such as eddies and oceanic fronts also play a vital role in redistributing ocean characteristics and associated biological responses (Bruce et al., 1994; Vipin et al., 2015; Sarma et al., 2018; Kurian et al., 2020).

Mesoscale eddies and fronts are known to supply nutrients to the euphotic zone, resulting in high productivity (Falkowski et al., 1998; Gruber et al., 2006; Vipin et al., 2015; Roy et al., 2015). Eddies are nonlinear mesoscale features of the oceanic circulation. They play a vital role in the vertical and horizontal transport of physical, chemical, and biological properties of the ocean (Klein and Lapeyre, 2009), whereas oceanic fronts are regions of enhanced surface gradients in physicochemical parameters between adjacent water masses (Belkin & Cornillon, 2005; Belkin et al., 2009). Since these physical features help in nutrient pumping and high productivity, they can contribute considerably to carbon and nitrogen cycling. Earlier, Hansell and Peltzer (1998) reported the seasonal variations in primary production in the AS, that significantly influence the organic carbon (OC) concentration and its flux. The composition of the plankton community mainly affects OC in the open ocean, and its distribution is primarily controlled by vertical mixing and water-mass circulation (Hansell and Carlson, 2002). Therefore, apart from seasonally varying phytoplankton bloom, mesoscale features induced productivity is also crucial for the fate of OC fluxes and oxygen minimum zone in the AS.

Previously several studies from EAS documented biological implications related to SWM upwelling (Rajagopalan et al., 1992; Habeebrehman et al., 2008; Smitha et al., 2008; Gupta et al., 2016; Jagadeesan et al., 2017; Karnan et al., 2017), eddies (Rejomon et al., 2013; Shafeeque et al., 2021; Smitha et al., 2021) and fronts (Vipin et al., 2015; Roy et al., 2015; Sarma et al., 2018; Krishna et al., 2018; Kurian et al., 2020). However, many of these studies on upwelling and fronts were limited to the southeastern Arabian Sea (SEAS) and Northeastern Arabian Sea (NEAS) respectively. Although biological aspects of SWM upwelling and mesoscale features are studied from EAS, their combined

role in regulating the biological response has not been investigated. In the present study, we attempted to explain the different role of SWM upwelling, mesoscale eddies, and oceanic fronts in controlling the biological features over a wide latitudinal transect in the EAS during the late SWM of 2017. The spatial variations of physical and biogeochemical parameters in the study region during the sampling period are explained.

2. Materials and Method

2.1. Study Area and Sampling

The study area in the EAS covers a wide latitudinal transect from 8°N to 21°N along 68°E (Stations-II-1 to II-14 at 1° intervals) (Fig. 1). Sample collection and water column measurements were carried out onboard *R.V. Sindhu Sadhana* during the SWM of 2017 (11-19 September; SSD-041). A CTD (Sea Bird) was used to obtain the temperature, salinity, and dissolved oxygen (DO). Apparent oxygen utilization (AOU) is calculated using the equation of Garcia and Gordon (1992) based on the O₂' values of Benson and Krauss (1984) followed by Shetye et al., (2021). The sampling for biogeochemical parameters from discrete depths was carried out from Niskin bottles attached to the rosette sampler.

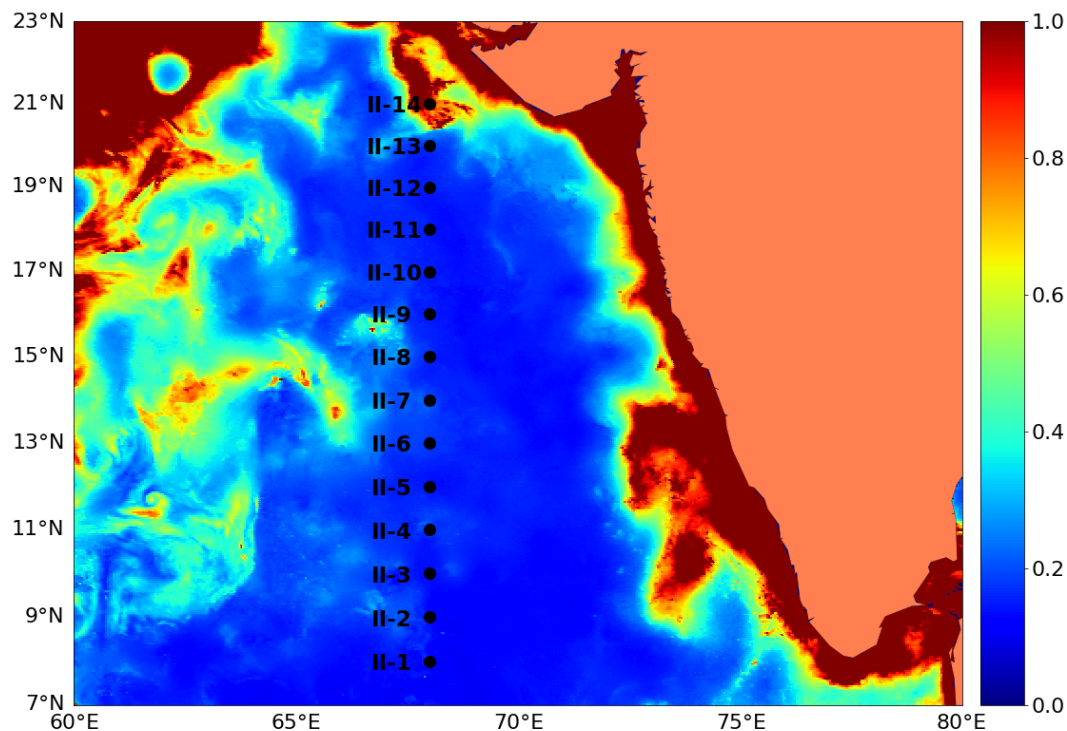


Figure. 1: Study area map showing the average of satellite-derived Chl-a concentration in mg m⁻³ (11-19 September 2017) and sampling locations with station numbers.

2.2 TOC and TN

Seawater for TOC and TN was analysed using Shimadzu TOC-LCPH coupled with a TN analyser. TOC was analysed at 680 °C following the catalytic combustion oxidation method (Dickson et al., 2007) and TN was analyzed at 720 °C using chemiluminescence method, wherein the oxidation product of nitrogen is quantified by reaction with ozone and detection of the resulting chemiluminescence (Badr et al., 2003; Letscher et al., 2013). The detailed methodology was explained by Shetye et al. (2021).

2.3 Chl-a and fucoxanthin analysis

2 L of water sample for Chl-a and fucoxanthin pigments was collected from discrete depths and straightaway filtered using a GF/F filter (0.7 µm; 25 mm) avoiding exposure to direct light and preserved at -80 °C until analysis. The frozen filters were extracted with 100% methanol, and analysed using high-performance liquid chromatography (Agilent Technologies) following the modified method of Van Heukelem (2002) as described in Kurian et al. (2012).

2.4. Total bacterial count analysis

50 ml of water sample for total bacterial count (TBC) was collected from discrete depths and fixed with 4% of 0.22 µm filtered formaldehyde and stored in the dark at 4 °C following the JGOFS Protocols (UNESCO, 1994). These samples were later filtered on black polycarbonate filters (0.2 µm, Nucleopore) and DAPI stained direct counts (AODC) were made. The total bacterial counting was done using Olympus BH2 epifluorescence microscope (Olympus Corp., Tokyo, Japan). The number of bacterial cells per liter was determined following Parsons et al. (1984).

2.5 Satellite-Derived Parameters

2.5.1 Sea Surface Level Anomaly (SLA):

The SLA is estimated by Optimal Interpolation, merging the measurement from the different altimeter missions available. Multiple satellite altimeters' (Jason-3, Sentinel-3A, HY-2A, Saral/AltiKa, Cryosat-2, Jason-2, Jason-1, T/P, ENVISAT, GFO, ERS1/2) merged product on SLA at a spatial resolution of 0.25°×0.25° were obtained from marine.copernicus. eu.

2.5.2. Chl- a:

Daily Chl-a data with a spatial resolution of 4 km × 4 km were downloaded from the marine.copernicus. eu (Garnesson et al., 2019). Products (Daily, Monthly, and Climatology) are based on merging the sensors SeaWiFS, MODIS, MERIS, VIIRS-SNPP&JPSS1, OLCI-S3A&S3B. For OLCI-S3A, products are also delivered as a single sensor.

2.5.3. Sea surface temperature (SST) fronts:

Daily SST data with a resolution of $1 \text{ km} \times 1 \text{ km}$ for the sampling period 10 September 2017 to 19 September 2017 were downloaded from the marine.copernicus. eu. The SST fronts were identified following the algorithm of Cayula and Cornillon (1992). We used a cutoff of 0.15°C to detect the fronts, as followed by Vipin et al. (2015) and Sarma et al. (2018).

2.6 ARMOR3D observational data

Weekly ARMOR3D observational data was downloaded from the marine.copernicus. eu. It is an observation based product consist of Temperature, Salinity, Heights, Geostrophic Currents and Mixed Layer Depth, available on a 0.25 degree regular grid and on 50 depth levels from the surface down to the bottom (Guinehut et al., 2012; Mulet, et al., 2012).

3. Results

3.1 Hydrography

The SST varied from a maximum of 28.9°C at station II-10 to a minimum of 28°C at II-6. Mixed Layer Depth (MLD) varied spatially through a deep MLD in the southern stations with a maximum depth of 47m at II-3, whereas a shallow MLD was observed at station II-8 (10 m deep). A shoaled isotherm was observed from the vertical distribution at stations II-6, II-10, and II-14 (Fig. 2 a). At these stations, 28°C isotherm was observed at 24 m compared to the other stations where the isotherm was much deeper. The salinity of these stations (II-6, II-10, and II-14) was low compared to the adjacent stations (Fig. 2 b). The entire water column from surface to 100m at southern station II-1 showed a low salinity compared to northern stations. Density varied from 23.18 kg/m^3 to 25.48 kg/m^3 in 100m water column with low values in the surface waters of II-8 to higher values at 100 m depth at II-14 (Fig.2 c). Consistent with salinity, low-density waters were observed in the 20 m water column of stations II-4, II-5, II-6, and II-8, and in the entire water column of station II-1. In II-12, the salinity and density were higher compared to other stations. The 100m water column was well oxygenated with DO concentrations varying from 1 mL/L to 4.5 mL/L (Fig.2 d). DO concentrations were $>4\text{mL/L}$ in the upper 60m for the southern stations, while it shoaled in the northern most station, II-14.

A high DO concentration is also observed at 80 to 100m water column of station II-8 compared to other stations.

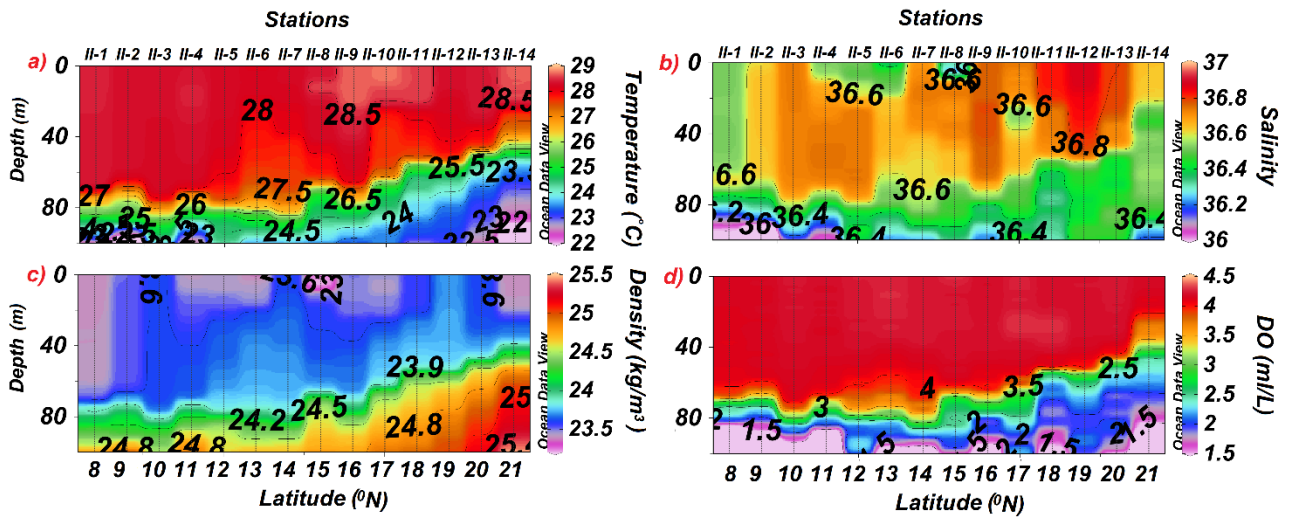


Figure. 2: Spatial and vertical variations of a) Temperature, b) Salinity c) Density and d) Dissolved Oxygen in the upper 100m water column along the 68°E in the EAS.

3.2 Spatial variations of biogeochemical parameters

TOC showed latitudinal variations in the upper oceanic water column with higher concentrations in the northern stations compared to the southern (Fig. 3 a). TOC varied from 62 to 120 μM in the 100 m water column with an average value of $81 \pm 13.6 \mu\text{M}$. The station II-14 showed a high concentration of TOC with an average value of $87 \pm 19.7 \mu\text{M}$, whereas the lowest concentration was observed at station II-6 with an average value of $74 \pm 11.6 \mu\text{M}$. Chl-a varied from below detection limit (BDL) to 0.371 $\mu\text{g/L}$ with a depth wise average concentration of $0.085 \pm 0.077 \mu\text{g/L}$ in the 100 m column of the transect (Fig. 3 b). The highest Chl-a concentration of 0.371 $\mu\text{g/L}$ was observed at surface of station II-14 followed by a concentration of 0.326 $\mu\text{g/L}$ at 20m of station II-14. A Chl-a maximum of 0.278 $\mu\text{g/L}$ was also observed at 54m of station II-13.. Interestingly, stations II-7 and II-8 displayed high Chl-a from surface to 70 m depth with Chl-a maximum at 54m (0.211 $\mu\text{g/L}$) and 70m (0.242 $\mu\text{g/L}$) respectively.. TBC varied from $0.2176 \times 10^9 \text{ cells /L}$ to $1.1454 \times 10^9 \text{ cells /L}$ in the 100 m column with higher counts at northern stations of the transect. (Fig. 3 c). The highest count of $1.1454 \times 10^9 \text{ cells /L}$ was observed at surface of Station II-14, whereas, 20 to 100m water column showed low TBC. Station II-8 exhibited low TBC in the entire 100m column with an average count of $0.292 \pm 0.024 \times 10^9 \text{ cells /L}$, while station II-9 showed a maximum count with an average value of $0.699 \pm 0.102 \times 10^9 \text{ cells /L}$.

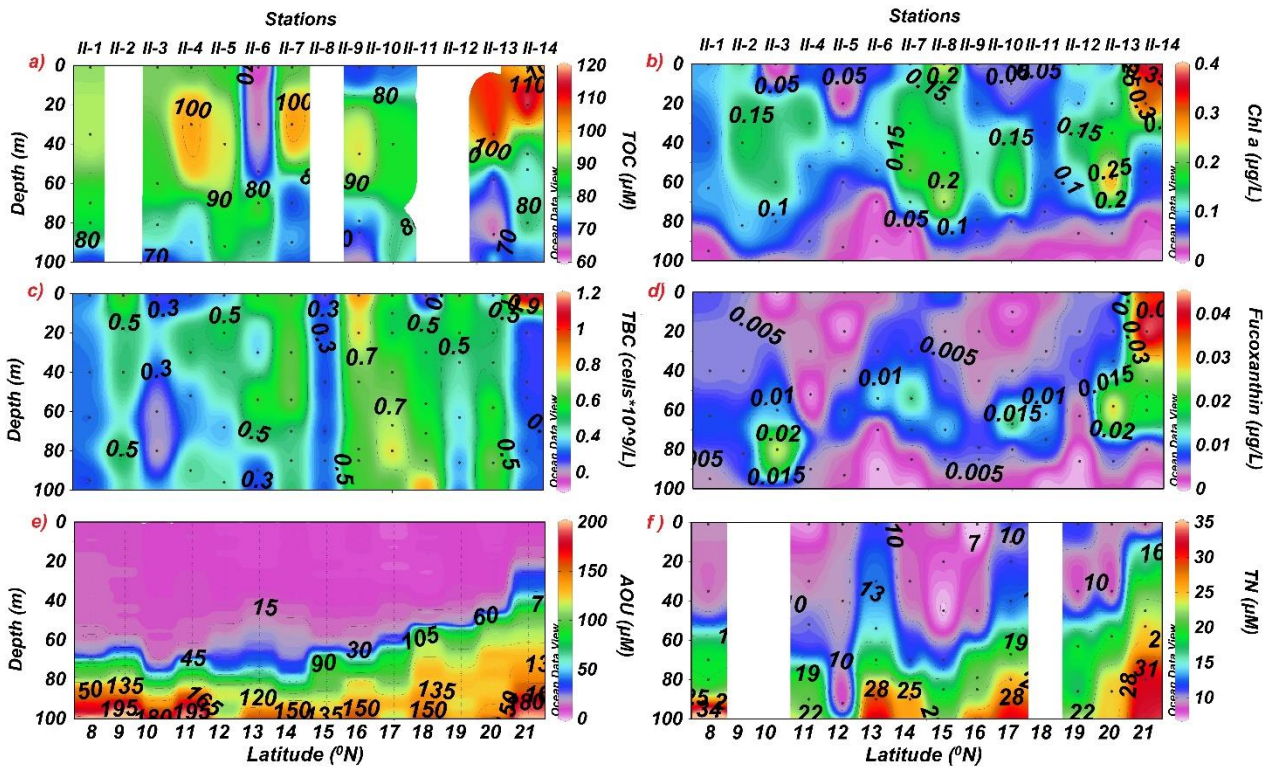


Figure. 3: Spatial and vertical distributions of a) TOC, b) Chl-a, c) TBC, d) Fucoxanthin, e) AOU and f) TN in upper 100m water column along the 68°E in the EAS.

Fucoxanthin showed a high concentration of $0.044 \mu\text{g/L}$ and $0.037 \mu\text{g/L}$ at the sub surface (20m) and surface of station II-14, respectively. (Fig. 3 d). It varied from BDL to $0.044 \mu\text{g/L}$ in the 100 m column with a high concentration at station II-14 (average of $0.021 \pm 0.016 \mu\text{g/L}$). Apart from station II-14, a fucoxanthin maximum concentration of $0.03 \mu\text{g/L}$ was also observed at 54m of station II-13.. AOU varied from $6.3 \mu\text{M}$ on the surface to $209.8 \mu\text{M}$ at 100m of the water column (Fig.3 e). TN showed a clear up sloping in stations II-6, II-10, and II-14 by vertical mixing of higher TN from the bottom waters to the subsurface and surface (Fig. 3 f). The average concentrations of TN for 100m column at these stations were $19.96 \pm 8.87 \mu\text{M}$, while at other stations, it was found to be $16 \pm 8.52 \mu\text{M}$. A higher column integrated Chl-a was shown in northern stations II-13 and II-14, central stations II-7 and II-8, and southern station II-2 (Fig. 4). The highest column integrated Chl-a was observed at station II-8 (15.9 mg/m^2) followed by II-13 (14.4 mg/m^2), II-14 (13.9 mg/m^2), II-2 (13.7 mg/m^2) and II-7 (12.1 mg/m^2).

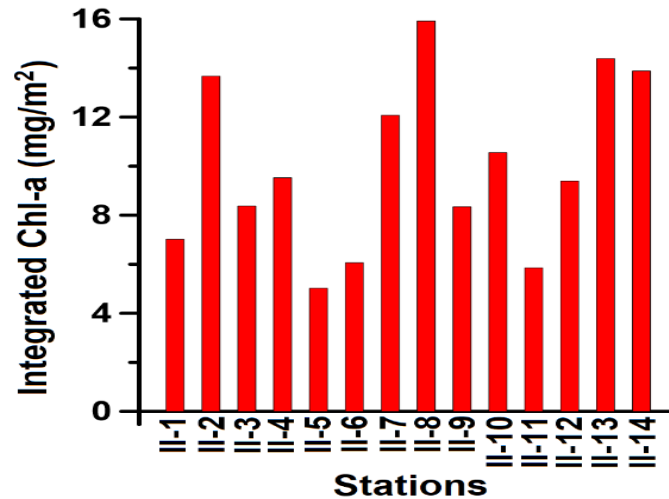


Figure.4. Integrated Chl-a concentrations in the 100m water column of EAS along 68 °E .

4. Discussion

Marine phytoplankton play a crucial role in regulating ecosystem functions, sustaining high fisheries, climatic processes, and biogeochemical cycles (Sebine et al., 2004, Chassot et al., 2010). Globally, primary production by phytoplankton is limited by light and nutrient supply in the ocean (Geider et al., 2001; Arrigo, 2005; Moore et al., 2013). Several studies have documented the limitations of nutrients, including silicate, nitrogen and iron (Burckle, 1989; Morrison et al., 1998; Koné et al., 2009; Naqvi et al., 2010; Moffett et al., 2015; Schoffman et al., 2016; Anju et al., 2020; Shetye et al., 2023) in the AS. The availability of nutrients in the oceans and their means of supply varies considerably from one region to another, mainly due to physical processes.

In the present study, we have measured the in-situ physicochemical parameters and associated biological changes in the 100m water column of a wide latitudinal transect along EAS. The in-situ measurements revealed distinct features from the study area. Firstly, vertical mixing occurred at stations II-6, and II-10, bringing cool, low saline, and nutrient-rich water from deeper depths to the sub-surface and surface (Fig. 2 a, b, and Fig. 3f). Secondly, based on integrated Chl-a values high biomass was observed in the northern stations II-13 and II-14, central stations II-7 and II-8 and the southern station II-2 (Fig.4). Apart from that a shoaling of thermocline is also observed towards northern stations with the shallowest MLD at station II-14. This feature is clearly visible from the low MLD toward north compared to the southern stations.

The vertical mixing at stations II-6, and II-10 is evident from the upshift of 28 °C isotherm to 24 m, salinity variation from adjacent stations, and supply of nutrient-rich waters to the subsurface and surface layers at these stations as seen from TN data. A slight uplift in AOU also observed in these

station. Although the same features are also observed at the Station II-14, the biological response in these stations are contrasting as high biomass is seen at station II-14 from the high concentration of Chl-a, TOC, and fucoxanthin, whereas station II-6 reported the lowest values of Chl-a and TOC. Increased biomass at II-2, II-7, II-8, II-13, and II-14 are also seen from high concentrations of TOC and fucoxanthin. To substantiate the in situ data and understand the dynamics in physical properties, we have compared the in situ data with ARMOR3D observational data and BioArgo data in the study area.

4.1 Comparison of insitu data with BioArgo data Armor3D observational data

ARMOR3D is an observation-based product by combining satellite SLA, SST, SSS datasets with in situ vertical profiles of temperature and salinity in order to build a global 3D weekly salinity, temperature, and geostrophic velocities fields at a spatial 0.25° resolution (Verbrugge et al., 2017). We have analysed the ARMOR3D data for temperature and salinity in the study area from June to September. The weekly average of temperature and salinity for the study area from 27th August to 23rd September is plotted to compare with in situ data, which is available from 11th to 19th September 2017 (Fig. 5). ARMOR3D is a weekly data set centered on Wednesday, so the average of 13th and 20th September data set is the average of data set from 10th to 23rd September 2017. The in situ temperature and salinity (Fig. 2 a and b) profiles are exactly matching with the temperature and salinity profiles of ARMOR3D during the weekly average of 13th and 20th September (Fig. 5 c,d,g, and h). The signature of vertical mixing in stations II-6 and II-10 is clearly visible in those two weeks. Although the signature of vertical mixing at II-6 was not seen during the previous week, at II-10, it is presented in the weekly average of 6th September. The temperature profiles from June to September clearly show an advection of cool water from north to south from July to September and warm water from the first week of September (Fig. S1).

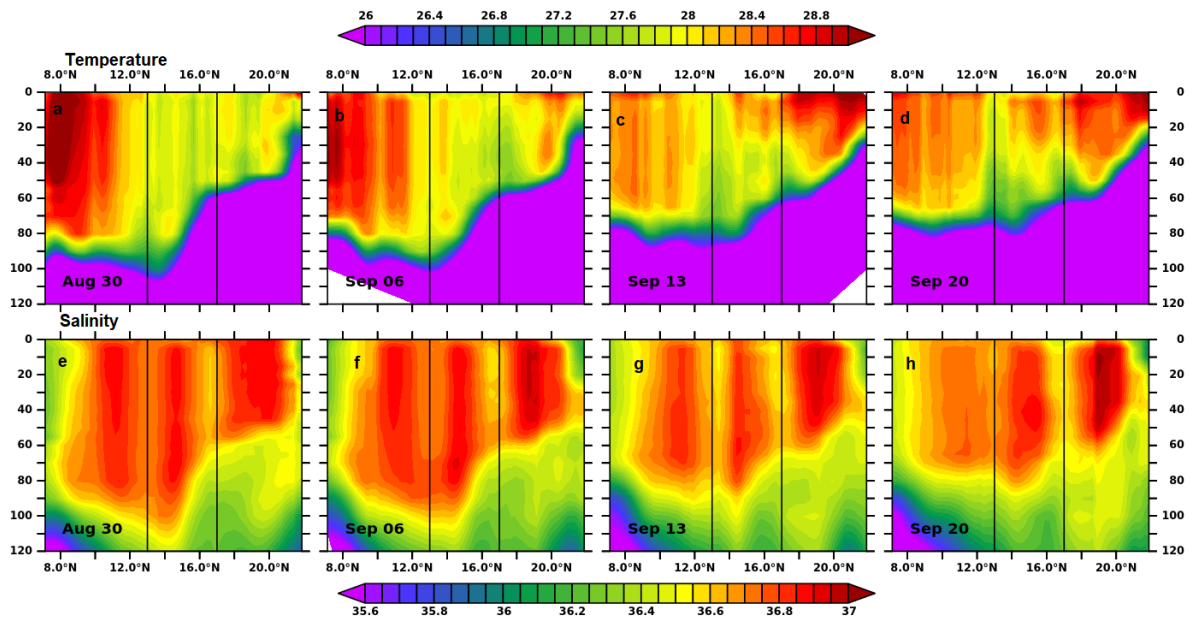


Figure 5: The weekly average of ARMOR3D data of a-d) temperature (°C) and e-h) Salinity from 27th August to 23rd September along the 68°E in the EAS. The black line represent the stations II-6 (13 °N) and II-10 (17 °N).

To make the in situ data more concrete, we have also compared with available Bio Argo data in the location during the sampling period. Although we didn't get the Bio Argo at the exact station locations, we have plotted the data available in the nearby locations of the stations (Bio Argo data locations and dates are given in the supplementary table 1). Shoaling Temperature contours and salinity observed at station II-10 (Fig. 6 a and c) is showing exactly the same signature of in situ data (Fig. 2 a and b). High Chl-a biomass in the station II-13 and II-8 (Fig. 6 b) are also observed in the insitu data along with high DO in the 80 to 100 m of II-8 (F ig. 6d). Thus, the features in the in situ data are very much comparable with the bio arago data and ARMOR3D observational data and is also explained clearly about the period of vertical mixing in the particular stations. So to understand the plausible reasons for the vertical mixing at stations II-6 and II-10 and high biomass at stations II-2, II-7, II-8, II-13, and II-14, we analyzed the mesoscale features and physical properties in the AS during the sampling period.

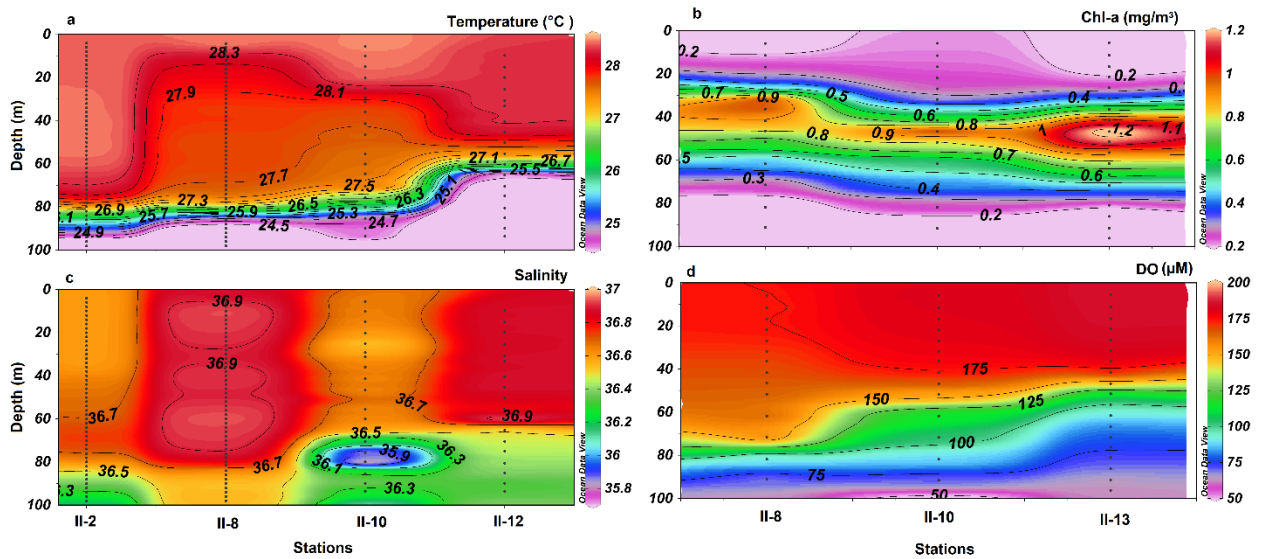


Figure 6: The Bio Argo data of a) temperature b) Chl-a c) Salinity, and d) DO in the 100m water columns of nearby locations of stations along the 68°E in the EAS.

4.2 Role of mesoscale eddies in the study region

4.2.1 Influence of mesoscale eddies in vertical mixing

Earlier, many studies have documented the increase in phytoplankton biomass through vertical mixing caused by the mesoscale eddies in the AS (Bruce et al., 1994; McCreary et al., 1996; Subrahmanyam and Robinson2000; Prasanna Kumar et al. 2000; Wiggert et al. 2005; Shafeeque et al., 2021; Smitha et al., 2021). To understand the role of mesoscale eddies in the vertical mixing in the study region, we examined the Sea LevelAnomaly (SLA) during the sampling period (11-19 September 2017) (Fig.7). The ring-shaped negative SLA are interpreted as cyclonic eddies, whereas positive SLA reflects the anticyclonic eddies. Cyclonic eddies increase productivity by upward injection of nutrients into the surface and subsurface waters (Falkowski et al., 1991; McGillicuddy et al., 1998; Klein and Lapeyre, 2009). While, anticyclonic eddies suppress primary production due to the downward motion resulting in the depletion of nutrients in the surface waters (McGillicuddy and Robinson, 1997; Sweeney et al., 2003). From figure 7, it is evident that the eddy fields do not influence the study region. Therefore vertical mixing at the stations II-6, II-10, and II-14 may not be due to the influence of mesoscale eddies.

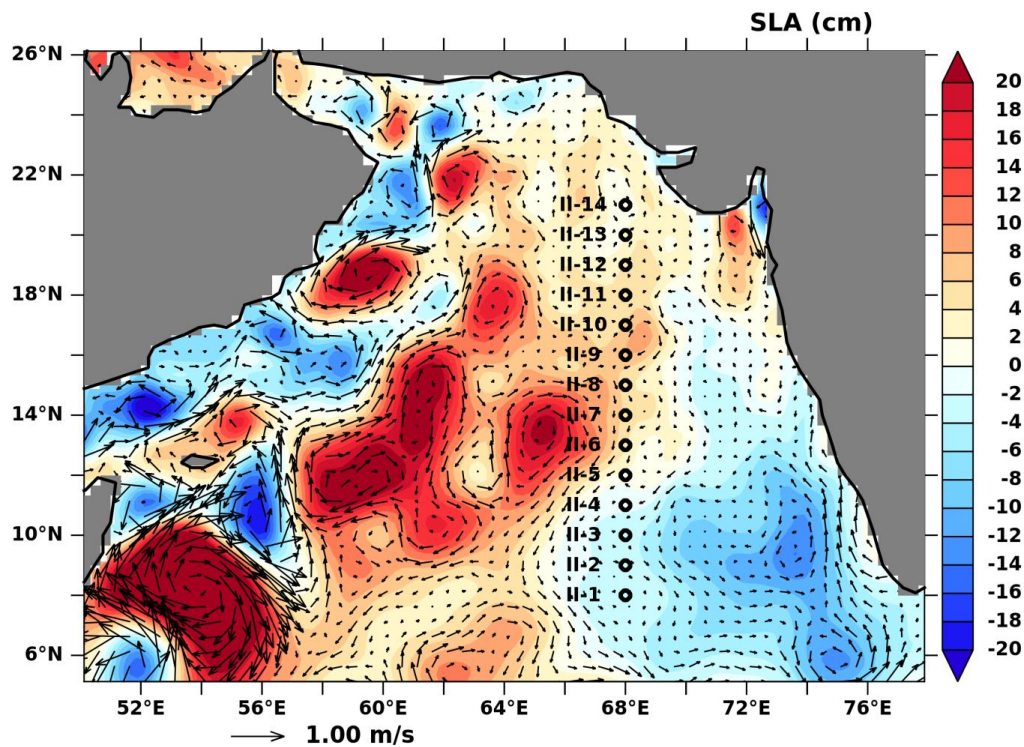


Figure 7: The average sea level anomaly with sea surface currents (m s^{-1}) during 11-19 September 2017 in the EAS.

However, there are many mesoscale eddies (cyclonic and anticyclonic) located in the AS, especially WAS and central Arabian sea (CAS), during the sampling period (Fig.7).

4.2.2 Lateral advection by eddies

The WAS displays a highly active eddy field during the SWM season (Trott et al., 2018), and their formations are induced by Findlater-Jet, coastal upwelling, and barotropic instabilities (McCreary et al., 1993; Trott et al., 2017). Besides the wind-induced coastal upwelling, mesoscale eddies also drive nutrients supply (Marra and Barber, 2005, Resplandy et al., 2011), hence productivity in the WAS. Earlier studies showed that the lateral advection prompted by eddies accounts for 50–70% of the total supply of nutrients to the central AS (Resplandy et al., 2011). Lateral advection supplies nutrients in the same order of magnitude as that of vertical advection.

The present study found numerous eddy fields in the WAS extending up to CAS during the sampling period (Fig. 7). To understand the role of these eddies in lateral advection, we have analyzed the weekly average of Chl-a along with the current in the AS from the first week of August to the third week of September (Fig. 8). Figure 8 showed a clear advection of Chl-a from the WAS to the study region,

especially near stations II-7 and II-8. Although the advection of Chl-a was observed during the sampling period, the maximum intensity of advection was seen during the mid of August (Fig.8). Earlier Resplandy et al. (2011) showed that eddy-induced lateral advection carries the nutrients from WAS to CAS through filamentary structures. Advection of upwelled nutrient-rich water to the CAS and associated productivity is also reported by many other studies (Prasanna Kumar et al., 2001; Joseph et al., 2019). Therefore the high biomass found in stations II-7, and II-8 might be due to eddy-induced advection of productive water mass from the WAS to the study region. Despite the earlier reports of eddy-induced advection to CAS, the present study suggested that eddy-induced lateral advection can transport nutrient-rich productive water from WAS to EAS. In order to understand the yearly changes in the advection, we have also analysed the monthly average of Chl-a along with the current in the AS from June to September of 2016 (Fig. S2). It is evidently clear that advection of high biomass from WAS to the study region occurring in 2016 also though its intensity less compared to 2017.

Resplandy et al., (2012) suggested that mesoscale filaments extending ~ 500–1000 km offshore redistribute the oxygenated waters along the western coast of the Arabian Sea brought by the Somali Current. Earlier McCreary et al. (2013) found that horizontal mixing connected with eddies is not needed to resolve the OMZ, which is in contradiction with the finding of Resplandy et al. (2012) who suggested the eddy-driven horizontal advection to be a crucial process in providing oxygen to the western central Arabian Sea and the southwestern Indian coast. Our results are in support of Resplandy et al. (2012) and indicate that lateral advection associated with eddies play an important role in transporting dissolved oxygen to the central and eastern Arabian Sea as the 80-100m waters of II-8 are having high dissolved oxygen compared to other stations (fig. 2 b).

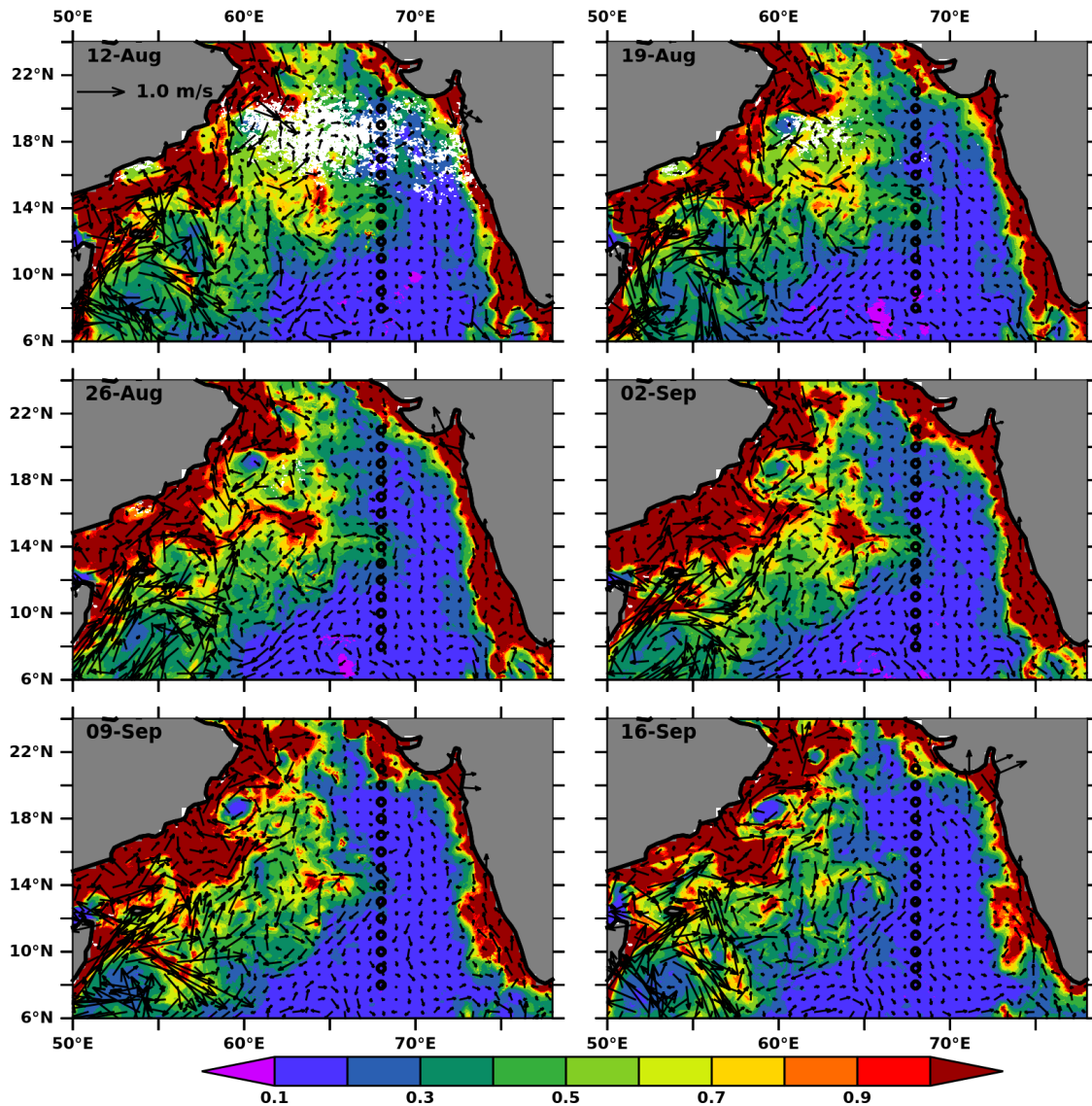


Figure 8: The weekly average Chl-a (mg m^{-3}) concentrations with sea surface currents (m s^{-1}) from 12th August to 16th September 2017 in the AS.

4.3. Influence of oceanic fronts on vertical mixing

Another vital feature of the ocean which can cause vertical mixing of relatively cool and nutrient-rich deep water with that of the surface is oceanic fronts (Pollard & Regier, 1990; Rudnick & Luyten, 1996; Vipin et al., 2015). Although horizontal gradients of temperature fronts in the NEAS are weaker than the subtropical and temperate regions, they are strong enough for vertical mixing (Vipin et al., 2015). To understand the influence of oceanic fronts in the study area, we analyzed daily images of SST data from 10 to 19th September 2017 (sampling period) using the single-image-edge-detection algorithm of

Cayula and Cornillion (1992) as detailed in Vipin et al. (2015) (Fig.9). Figure 9 showed that frontal features were present at stations II-6 and II-10 during the sampling period.

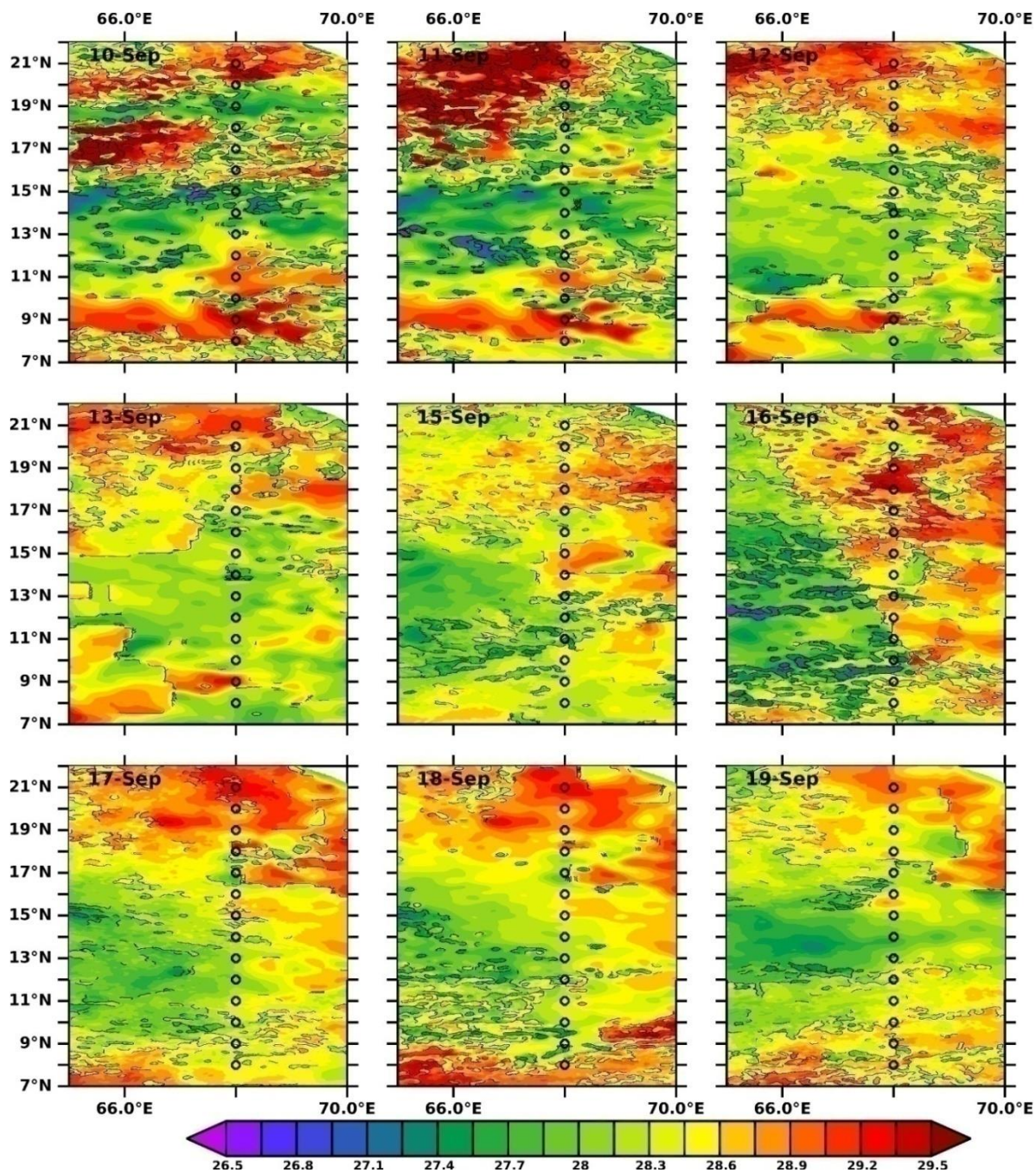


Figure 9: Satellite-derived SST (°C) and fronts (detected by the single-image-edge-detection algorithm) in the EAS from 10-19 September 2017. Black circles represent station locations, the color bar represents the SST, and the contours represent the fronts.

In the present study, the stations II-6, and II-10, were sampled on the 14th, and 16th of September 2017, respectively. Fronts were observed at stations II-6 and II-10 on 15th September (Fig.7). At station II-10, the front was formed on the previous day of the sampling (15th September), while at II-6 front was

not present on the previous day. Since the SST data was unavailable on 14th September, we assume that the front seen on 15th September might have formed on 14th September (sampling day) at II-6. At station II-6, we assumed that a front having short life appeared on 14th and disappeared on 16th September (no SST data available for 14th September) (Fig.10 a). While at station II-10, the front was detected on 15th September and lasted until 18th September (Fig.10 b).

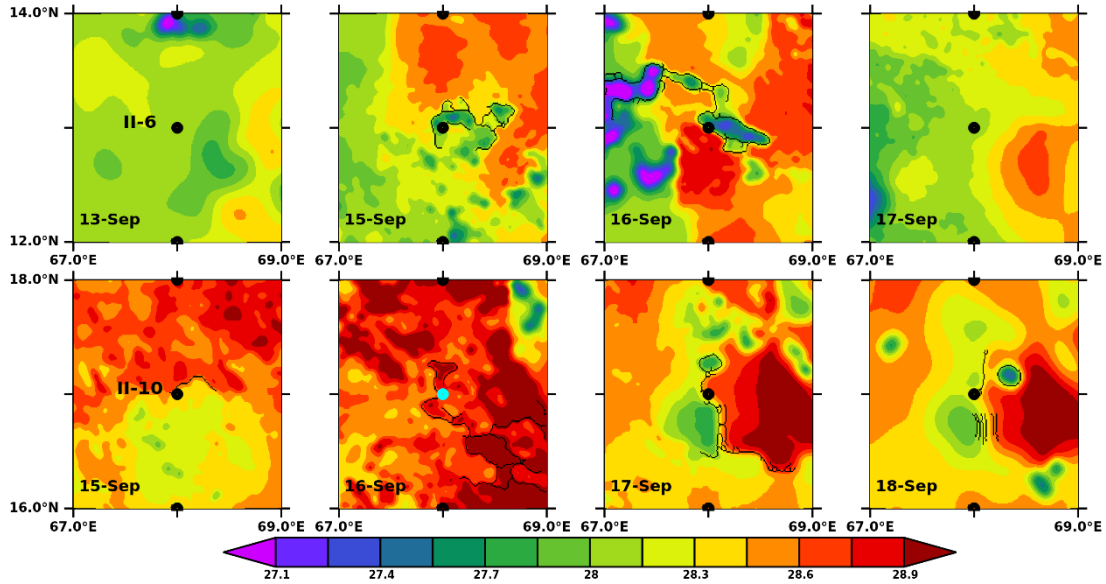


Figure 10: Zoomed images of SST (°C) fronts at stations II-6 (top) and II-10 (bottom). The black dots represent the station, and the blue dot represents the sampling day (II-6 was sampled on 14th September and the data was not available).

Figure 11 a and b show the weekly averaged ARMOR3D temperature profiles on 6th and 13th September 2017. The vertical uplift of 27.75 °C from ~70 m at 12 °N to ~40 m at 13 °N on 13th September (data is averaged from 10 -16 September) is observed at station II-6, where we observed front on 15th September. At 17 °N, station II-10 shows a slight uplift of 27.75 °C isotherm at ~20m on 6th September (weekly averaged from 3- 9 September). By 13th September, because of the advection of warm waters from the north the 27.75°C isotherm is seen only till ~40m. Apart from these 2 frontal zones at station II-6 and II-10, where vertical mixing is indicated by the isotherms upliftment, in general the shoaling of isotherm is also observed to north of 14 °N. We use 27.75°C isotherm to indicate this possible vertical mixing in the frontal zones. To verify this vertical mixing and upliftment of isotherms we calculated the barotropic and baroclinic instabilities (Fig. 11 c-f).

The instabilities were calculated using energy conversion terms following (Chen et al. 2018), Mukherjee et al., 2017). The barotropic conversion term (E_{BT}) and baroclinic conversion (E_{BC}) terms are given by

$$E_{BT} = - \left\{ u' u' \frac{\partial \bar{u}}{\partial x} + u' v' \left(\frac{\partial \bar{v}}{\partial x} + \frac{\partial \bar{u}}{\partial y} \right) + v' v' \frac{\partial \bar{v}}{\partial y} \right\}$$

$$E_{BC} = \frac{-g}{\rho \left(\frac{\partial \rho_\theta}{\partial z} \right)} \left(u' \rho' \frac{\partial \bar{\rho}}{\partial x} + v' \rho' \frac{\partial \bar{\rho}}{\partial y} \right)$$

where ρ_θ is the time and horizontal mean potential density in the Arabian Sea; $\rho' = \rho - \bar{\rho}$, $u' = u - \bar{u}$, and $v' = v - \bar{v}$; $\bar{\rho}$ is the time mean density and \bar{u} and \bar{v} are the zonal and meridional components of mean current.

High instabilities values indicate that the system grows by extracting energy from the mean flow (Mukherjee et al., 2017). Positive E_{BT} implies that part of the kinetic energy of the mean flow is converted to eddy kinetic energy. Positive E_{BC} indicates the mean available potential energy is converted to eddy potential energy (chen et al., 2018). Baroclinic instabilities indicate higher vertical shear and the barotropic instabilities indicate higher horizontal shear.

On 6th September, the instabilities are higher north of 15°N, particularly in the top 60m of the water column. The higher instabilities sustained till 13th September and more prominently observed to the 17°N. The barotropic instability is weakened slightly from 6th September to 13th September, however it remained higher compared to southern latitudes (Fig11 e and f). Thus the vertical mixing observed at the stations II-6 and II-10 are might be due to the associated higher instabilities and oceanic fronts.

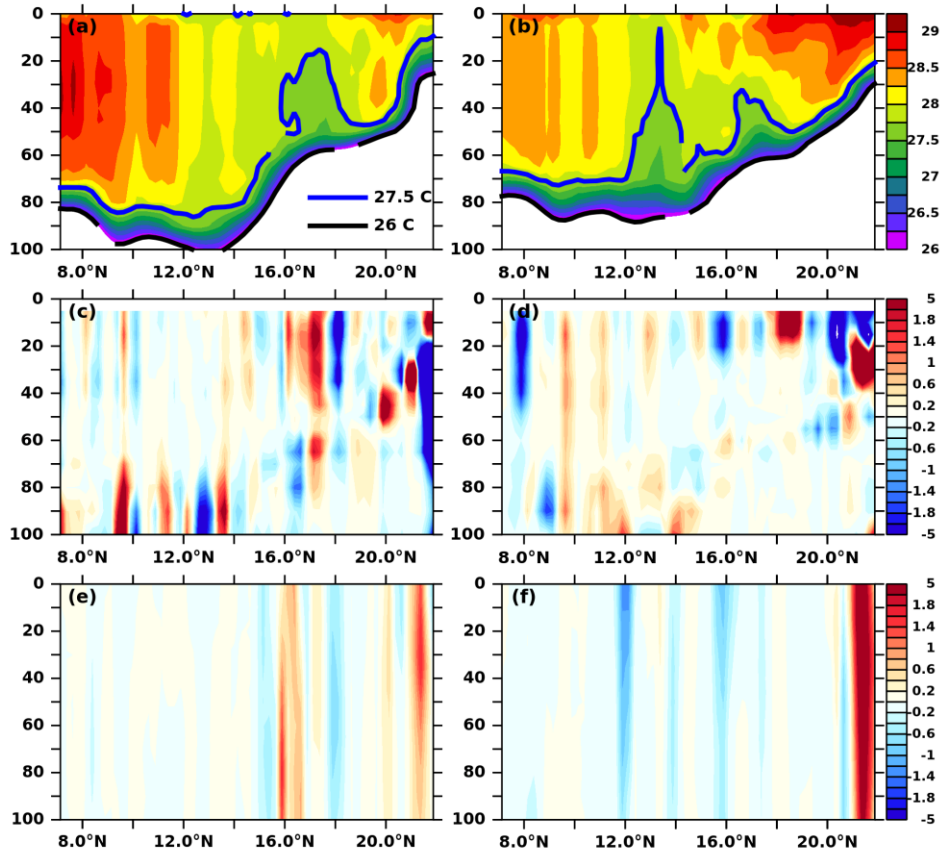


Figure 11: a) and b) ARMOR3D weekly average temperature ($^{\circ}\text{C}$) profile on 06th and 13th September 2017; c) and d) baroclinic instability (E_{BC} , $10^{-5} \text{ cm}^2 \text{ s}^{-3}$) for 6th and 13th September 2017; e) and f) barotropic instability (E_{BT} , $10^{-5} \text{ cm}^2 \text{ s}^{-3}$) for 6th and 13th September 2017. The black and blue contour in (a) and (b) refers to 26 $^{\circ}\text{C}$ and 27.75 $^{\circ}\text{C}$ isotherm respectively.

4.3.1. Variations in biological responses at station II-6 and II-10

The ecosystem response to the availability of nutrients in a frontal system is complex because the lag in biological response in the frontal regime depends on the trophic level and varies across species within each trophic level (Sarma et al., 2018). However, many studies from the NEAS showed high phytoplankton production in the frontal zone (Roy et al., 2015; Sarma et al., 2015, 2018; Krishna et al., 2018). Recently, Kurian et al. (2020) also showed high phytoplankton biomass contributed by the open-ocean front, which occurred two days before the sampling at station II-8. Their study was also carried out in the same region during the late SWM (September - October) of 2014. Since the front was formed in the day of sampling and vertical mixing was observed in the weekly average of temperature on 13th September (10-17 September), the biological response in the II-6 is low compared to II-10. Although the front was seen on 15th September, we could see a vertical mixing and higher instability in the ARMOR3D weekly average data of 6th September (Fig. 11). This might be led to the

higher biological response in II-10 as seen from high integrated Chl-a, and TOC than II-6 (Fig. 4 and 3a).

4.4. Role of SWM upwelling in the study region

EAS located along the west continental margin of Indian subcontinent experiences intense monsoon induced upwelling during SWM (Smitha et al., 2008; Shah et al., 2015) and significantly high plankton productivity along the west coast of India (Banse, 1959; Gupta et al., 2016; Albin et al., 2022). Earlier studies reported that high intensity of upwelling is limited to SEAS (Banse, 1959; Shetye et al., 1990; Habeebrehman et al., 2008). However, Albin et al., (2022) reported coastal upwelling along the entire western shelf of the EAS with varying intensities. The shoaling of thermocline towards northern station and high Chl-a biomass at station II-13 and II-14 might be due to the effect of monsoon upwelling as the figure 2 also showed an upwelling signature towards northern stations.. A positive Ekman pumping velocity showed in the northern stations during June to august indicate upwelling in these region as positive Ekman pumping velocity is used as an index for upwelling (Fig. 12). Thus shoaling of thermocline started from July is due to the wind induced upwelling and is strengthened and persists during July to September (Fig. S1). Moreover, the northern stations are located towards coast and which would strengthen the upwelling intensity and shoaling of thermocline. Satellite derived Chl a in the present study also demonstrated upwelling induced high productivity over the western shelf of EAS (Fig.1 and Fig.8). From figure 1 and 8, it is clear that station II-13 and II-14 are highly productive regions induced by monsoon upwelling, which led to the high Chl-a biomass in those stations.

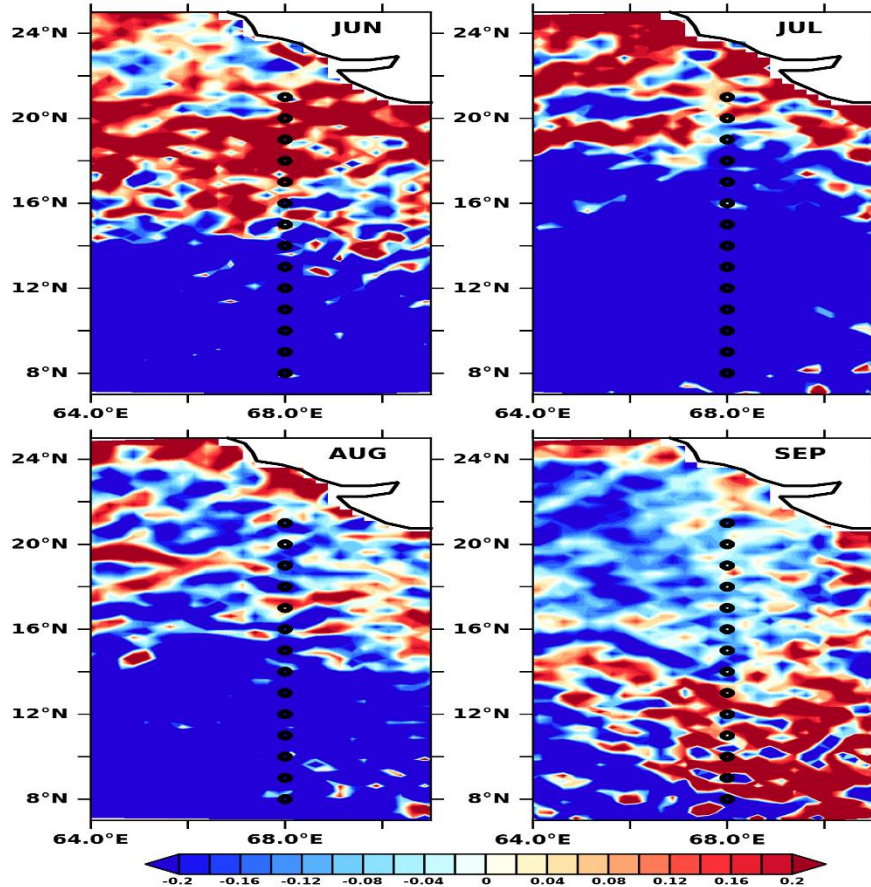


Figure 12: Ekman pumping velocity (10^{-5} ms^{-1}) from June to September of 2017 in the study region.

4.5. Significance of mesoscale features in regulating the biological responses

Upwelling systems are going to change in future with possible reduction in upwelling in the northern hemisphere (Chang et al., 2023). Therefore there is a need to understand how ocean biogeochemistry and fisheries will be impacted by upwelling and other physical processes. The role of upwelling and large-scale along coast advection anomalies is well known and they are reported to be equally important in changing shelf water properties (Stone et al., 2018). However, there still exist scarcity with respect to the role of lateral advection in influencing biogeochemistry of open oceanic waters. From the present study it is clear that the lateral advection from eddies not only supplies nutrients but also transports Chl a to the open eastern Arabian Sea waters far from its origin. The important highlight is that the integrated Chl a at station II-8 is higher than at station II- 14, although surface waters of II- 14 are having very high Chl a as compared to surface waters at II- 8. From this finding we can decipher that although southwest monsoon driven upwelling supplies nutrients within the top 100m, it also supplies low Chl a waters from the subsurface, while the eddy driven advection supplies high Chl a waters throughout the 100m, thus making the station II-8 more biologically productive. This is than

reflected on the biological communities also, wherein despite high Chl a and TOC at the surface waters, the TBC at II-14 below surface waters is very low. High Chl a throughout the top 100m s can have several implications including having a negative feedback towards climate change. Apart from that the lateral advection from eddies is also supplying oxygen rich waters to the upper boundary of the oxygen minimum zone. This can have inhibitory role on the ongoing expansion and intensification of the Arabian Sea oxygen minimum zones. In contrary to this, recently, Shetye et al. (2021) suggested that high TOC in the eastern Arabian Sea transported from the Gulf region can cause the expansion of OMZ in the eastern Arabian Sea. However, the difference being that in the present study the advected water not only has higher organic matter, it also has high dissolved oxygen. Eddy associated productivity and a resultant higher rate of organic carbon fluxes to the deeper layers are noticed from sediment traps measurements in the Arabian Sea (Honjo et al., 1999; Marra and Barber, 2005; Wiggert et al., 2005). Also, increased eddy mixing was responsible for the 70% of biogenic sedimentation noted from the sediment trap studies (Nair *et al.*, 1989; Haake *et al.*, 1993; Wiggert *et al.*, 2005). High productivity will also play a key role in regulating fish landings, eg. High oil sardines associated with nutrients and organic matter during 2017 in the eastern Arabian Sea. (Shetye et al., 2019).

The enriched productions by eddies and fronts is known to fascinate high migratory fish species (Braun et al., 2019) and form a key environment for fish larvae (Bécognée et al., 2009; Govoni et al., 2010). Apart from the identification of potential fishery zone (PFZ) using SST and Chl-a data (Solanki et al., 2003, 2010), Sarma et al. (2018) reported that an increase in integrated Chl-a in the frontal regime from the Arabian Sea can be used as a marker for PFZ. Since the advection of eddies is also responsible for the dispersal of fish larvae (Chang et al., 2017), the eddy-induced movement of phytoplankton biomass to EAS is very significant in the context of the present study.

Sarma et al. (2015) reported enhanced pCO₂ levels (by 3 to 50 µatm) within the fronts, suggesting that temperature fronts can be a source of atmospheric CO₂. Higher POC in the frontal region than that of the non-frontal area (Krishna et al., 2018) also suggest that the frontal zone can be a site of CO₂ fixation. These reports imply that fronts may play a vital role in carbon cycling, but the net effect is poorly understood. Recently, Stukel et al. (2017) reported that oceanic fronts enhance carbon export by gravitational flux (particle sinking) and subduction (water containing organic matter being forced downward) in the coastal waters of California. Enhanced fecal pellet production by mesozooplankton and consumption of silicon by diatoms are responsible for the increase in gravitational flux in the frontal zone (Stukel et al., 2017). However, microbial loops with increased total bacterial count (TBC) are more dominant in the open ocean fronts than the high zooplankton biomass in the inner shelf front (Sarma et al., 2018). Kurian et al. (2020) reported high TBC in the frontal zone than that of non-frontal

sites from the NEAS. This is consistent with the present study as the stations II-6 and II-10 showed high TBC in the 100m water column. Therefore the present study suggests that mesoscale eddy and front have important roles in shaping the biological productivity, associated carbon sequestration and its role in the sustenance of OMZ are significant and warrant attention.

5. Conclusion

Based on in-situ variability of biogeochemical parameters, observational data, and satellite data, a wide latitudinal transect in the EAS was studied during the late SWM of 2017. The observational data showed that oceanic fronts along with higher instabilities are responsible for the vertical mixing at stations II-6, and II-10. From the temperature, salinity, and TN data, these two stations showed an upshift of cold, low saline, and high nutrient water to the surface and sub-surface. The difference in time period of vertical mixing led to contrasting biological response in II-6 and II-10. Apart from this, the satellite chlorophyll data revealed that the eddy induced advection of productive water from WAS led to an increase in Chl-a and fucoxanthin pigments at stations II-7 and II-8. The study also found that SWM upwelling is responsible for the shoaling thermocline in the northern stations and increases phytoplankton biomass at northern stations II-13 and II-14. The study suggests that along with monsoon-related upwelling and productivity, eddies and fronts are also responsible for driving phytoplankton biomass in the EAS during SWM which can lead to higher carbon sequestration.

6. Acknowledgement

We thank the Director, CSIR- NIO for his support and encouragement. We are grateful to the scientific team on-board SSD 41 for their cooperation and support. We also thank Dr. Arnab Mukherjee for providing the codes for estimating baroclinic and barotropic instabilities. This study was carried out as a part of the projects PSC-0108 (INDIAS-IDEA) funded by CSIR, and GAP-2425 (SIBER-INDIA) funded by the Ministry of Earth Sciences, New Delhi. This is NIO contribution No:

References

1. Abernathey, R., Gnanadesikan, A., Pradal, M. A., & Sundermeyer, M. A. (2022). Isopycnal mixing. In *Ocean Mixing* (pp. 215-256). Elsevier.
2. Ajith Joseph, K., Jayaram, C., Nair, A., George, M. S., Balchand, A. N., & Pettersson, L. H. (2019). Remote sensing of upwelling in the Arabian Sea and adjacent near-coastal regions. In *Remote sensing of the Asian Seas*. Springer, Cham, 467-483.
3. Albin, K. J., Jyothibabu, R., Alok, K. T., Santhikrishnan, S., Sarath, S., Sudheesh, V., ... & Gupta, G. V. M. (2022). Distinctive phytoplankton size responses to the nutrient enrichment of coastal upwelling and winter convection in the eastern Arabian Sea. *Progress in Oceanography*, 203, 102779.

4. Anju, M., Sreeush, M. G., Valsala, V., Smitha, B. R., Hamza, F., Bharathi, G., & Naidu, C. V. (2020). Understanding the role of nutrient limitation on plankton biomass over Arabian Sea via 1-D coupled biogeochemical model and bio-Argo observations. *Journal of Geophysical Research: Oceans*, 125(6), e2019JC015502.
5. Arrigo, K. R. (2005). Marine microorganisms and global nutrient cycles. *Nature*, 437(7057), 349-355.
6. Badr, E. S. A., Achterberg, E. P., Tappin, A. D., Hill, S. J., & Braungardt, C. B. (2003). Determination of dissolved organic nitrogen in natural waters using high-temperature catalytic oxidation. *TrAC Trends in Analytical Chemistry*, 22(11), 819-827.
7. Banse, K. (1959). On upwelling and bottom-trawling off the southwest coast of India. *Journal of the Marine Biological Association of India*, 1(1), 33-49.
8. Bauer, S., Hitchcock, G. L., & Olson, D. B. (1991). Influence of monsoonally-forced Ekman dynamics upon surface layer depth and plankton biomass distribution in the Arabian Sea. *Deep Sea Research Part A. Oceanographic Research Papers*, 38(5), 531-553.
9. Bécognée, P., Moyano, M., Almeida, C., Rodríguez, J. M., Fraile-Nuez, E., Hernández-Guerra, A., & Hernández-León, S. (2009). Mesoscale distribution of clupeoid larvae in an upwelling filament trapped by a quasi-permanent cyclonic eddy off Northwest Africa. *Deep Sea Research Part I: Oceanographic Research Papers*, 56(3), 330-343.
10. Belkin, I. M., & Cornillon, P. C. (2005). Bering Sea thermal fronts from Pathfinder data: Seasonal and interannual variability. *Pacific Oceanography*, 3(1), 6-20.
11. Belkin, I. M., & O'Reilly, J. E. (2009). An algorithm for oceanic front detection in chlorophyll and SST satellite imagery. *Journal of Marine Systems*, 78(3), 319-326.
12. Benson, B. B., & Krause Jr, D. (1984). The concentration and isotopic fractionation of oxygen dissolved in freshwater and seawater in equilibrium with the atmosphere 1. *Limnology and oceanography*, 29(3), 620-632.
13. Boccaletti, G., Ferrari, R., & Fox-Kemper, B. (2007). Mixed layer instabilities and restratification. *Journal of Physical Oceanography*, 37(9), 2228-2250.
14. Braun, C. D., Gaube, P., Sinclair-Taylor, T. H., Skomal, G. B., & Thorrold, S. R. (2019). Mesoscale eddies release pelagic sharks from thermal constraints to foraging in the ocean twilight zone. *Proceedings of the National Academy of Sciences*, 116(35), 17187-17192.
15. Brock, J., Sathyendranath, S., & Platt, T. (1994). A model study of seasonal mixed-layer primary production in the Arabian Sea. *Proceedings of the Indian Academy of Sciences-Earth and Planetary Sciences*, 103(2), 163-176.
16. Bruce, J. G., Johnson, D. R., & Kindle, J. C. (1994). Evidence for eddy formation in the eastern Arabian Sea during the northeast monsoon. *Journal of Geophysical Research: Oceans*, 99(C4), 7651-7664.
17. Burckle, L. H. (1989). Distribution of diatoms in sediments of the northern Indian Ocean: Relationship to physical oceanography. *Marine Micropaleontology*, 15(1-2), 53-65.

18. Callies, J., & Ferrari, R. (2013). Interpreting energy and tracer spectra of upper-ocean turbulence in the submesoscale range (1–200 km). *Journal of Physical Oceanography*, 43(11), 2456-2474.
19. Cayula, J. F., & Cornillon, P. (1992). Edge detection algorithm for SST images. *Journal of atmospheric and oceanic technology*, 9(1), 67-80.
20. Chang, P., Xu, G., Kurian, J., Small, R. J., Danabasoglu, G., Yeager, S., ... & Chapman, P. (2023). Uncertain future of sustainable fisheries environment in eastern boundary upwelling zones under climate change. *Communications Earth & Environment*, 4(1), 19.
21. Chang, Y. L., Miyazawa, Y., & Beguer-Pon, M. (2017). The dynamical impact of mesoscale eddies on migration of Japanese eel larvae. *PloS one*, 12(3), e0172501.
22. Chassot, E., Bonhommeau, S., Dulvy, N. K., Mélin, F., Watson, R., Gascuel, D., & Le Pape, O. (2010). Global marine primary production constrains fisheries catches. *Ecology letters*, 13(4), 495-505.
23. Chen, G., Li, Y., Xie, Q., & Wang, D. (2018). Origins of eddy kinetic energy in the Bay of Bengal. *Journal of Geophysical Research: Oceans*, 123(3), 2097-2115.
24. Dickson, A. G., Sabine, C. L., & Christian, J. R. (2007). *Guide to best practices for ocean CO2 measurements*. North Pacific Marine Science Organization.
25. Falkowski, P. G., Barber, R. T., & Smetacek, V. (1998). Biogeochemical controls and feedbacks on ocean primary production. *science*, 281(5374), 200-206.
26. Falkowski, P. G., Ziemann, D., Kolber, Z., & Bienfang, P. K. (1991). Role of eddy pumping in enhancing primary production in the ocean. *Nature*, 352(6330), 55-58.
27. Fox-Kemper, B., Ferrari, R., & Hallberg, R. (2008). Parameterization of mixed layer eddies. Part I: Theory and diagnosis. *Journal of Physical Oceanography*, 38(6), 1145-1165.
28. Garcia, H. E., & Gordon, L. I. (1992). Oxygen solubility in seawater: Better fitting equations. *Limnology and oceanography*, 37(6), 1307-1312.
29. Garnesson, P., Mangin, A., Fanton d'Andon, O., Demaria, J., & Bretagnon, M. (2019). The CMEMS GlobColour chlorophyll a product based on satellite observation: Multi-sensor merging and flagging strategies. *Ocean Science*, 15(3), 819-830.
30. Geider, R. J., Delucia, E. H., Falkowski, P. G., Finzi, A. C., Grime, J. P., Grace, J., ... & Woodward, F. I. (2001). Primary productivity of planet earth: biological determinants and physical constraints in terrestrial and aquatic habitats. *Global change biology*, 7(8), 849-882.
31. Govoni, J. J., Hare, J. A., Davenport, E. D., Chen, M. H., & Marancik, K. E. (2010). Mesoscale, cyclonic eddies as larval fish habitat along the southeast United States shelf: a Lagrangian description of the zooplankton community. *ICES Journal of Marine Science*, 67(3), 403-411.
32. Gruber, N., Frenzel, H., Doney, S. C., Marchesiello, P., McWilliams, J. C., Moisan, J. R., ... & Stolzenbach, K. D. (2006). Eddy-resolving simulation of plankton ecosystem dynamics in the California Current System. *Deep Sea Research Part I: Oceanographic Research Papers*, 53(9), 1483-1516.

33. Guinehut, S., Dhomp, A. L., Larnicol, G., & Le Traon, P. Y. (2012). High resolution 3-D temperature and salinity fields derived from in situ and satellite observations. *Ocean Science*, 8(5), 845-857.
34. Gupta, G. V. M., Sudheesh, V., Sudharma, K. V., Saravanane, N., Dhanya, V., Dhanya, K. R., ... & Naqvi, S. W. A. (2016). Evolution to decay of upwelling and associated biogeochemistry over the southeastern Arabian Sea shelf. *Journal of Geophysical Research: Biogeosciences*, 121(1), 159-175.
35. Haake, B., Ittekkot, V., Rixen, T., Ramaswamy, V., Nair, R. R., & Curry, W. B. (1993). Seasonality and interannual variability of particle fluxes to the deep Arabian Sea. *Deep Sea Research Part I: Oceanographic Research Papers*, 40(7), 1323-1344.
36. Habeebrehman, H., Prabhakaran, M. P., Jacob, J., Sabu, P., Jayalakshmi, K. J., Achuthankutty, C. T., & Revichandran, C. (2008). Variability in biological responses influenced by upwelling events in the Eastern Arabian Sea. *Journal of Marine Systems*, 74(1-2), 545-560.
37. Hansell, D. A., & Carlson, C. A. (Eds.). (2014). *Biogeochemistry of marine dissolved organic matter*. Academic Press.
38. Hansell, D. A., & Peltzer, E. T. (1998). Spatial and temporal variations of total organic carbon in the Arabian Sea. *Deep Sea Research Part II: Topical Studies in Oceanography*, 45(10-11), 2171-2193.
39. Heukelem, Van, (2002). HPLC phytoplankton pigments: sampling, laboratory methods, and quality assurance procedures. *Ocean optics protocols for satellite ocean color sensor validation, revision*, 3(2), 258-268.
40. Honjo, S., Dymond, J., Prell, W., & Ittekkot, V. (1999). Monsoon-controlled export fluxes to the interior of the Arabian Sea. *Deep Sea Research Part II: Topical Studies in Oceanography*, 46(8-9), 1859-1902.
41. Jagadeesan, L., Jyothibabu, R., Arunpandi, N., Karnan, C., & Balachandran, K. K. (2017). Dominance of coastal upwelling over Mud Bank in shaping the mesozooplankton along the southwest coast of India during the Southwest Monsoon. *Progress in Oceanography*, 156, 252-275.
42. Karnan, C., Jyothibabu, R., Arunpandi, N., Albin, K. J., Parthasarathi, S., & Krishnan, S. S. (2020). Response of microplankton size structure to summer stratification, freshwater influx and coastal upwelling in the Southeastern Arabian Sea. *Continental Shelf Research*, 193, 104038.
43. Klein, P., & Lapeyre, G. (2009). The oceanic vertical pump induced by mesoscale and submesoscale turbulence. *Annu. Rev. Mar. Sci*, 1(1), 351-375.
44. Koné, V., Aumont, O., Lévy, M., & Resplandy, L. (2009). Physical and biogeochemical controls of the phytoplankton seasonal cycle in the Indian Ocean: A modeling study. *Indian Ocean Biogeochemical Processes and Ecological Variability*, 185, 350.
45. Krishna, M. S., Mukherjee, J., Dalabehera, H. B., & Sarma, V. V. S. S. (2018). Particulate organic carbon composition in temperature fronts of the northeastern Arabian Sea during winter. *Journal of Geophysical Research: Biogeosciences*, 123(2), 463-478.

46. Kumar, S. P., Madhupratap, M., Kumar, M. D., Gauns, M., Muraleedharan, P. M., Sarma, V. V. S. S., & De Souza, S. N. (2000). Physical control of primary productivity on a seasonal scale in central and eastern Arabian Sea. *Journal of Earth System Science*, 109(4), 433-441.
47. Kumar, S. P., Madhupratap, M., Kumar, M. D., Muraleedharan, P. M., De Souza, S. N., Gauns, M., & Sarma, V. V. S. S. (2001). High biological productivity in the central Arabian Sea during the
48. Kumar, S. P., Madhupratap, M., Kumar, M. D., Muraleedharan, P. M., De Souza, S. N., Gauns, M., & Sarma, V. V. S. S. (2001). High biological productivity in the central Arabian Sea during the summer monsoon driven by Ekman pumping and lateral advection. *Current Science*, 1633-1638.
49. Kurian, S., Chndrasekhararao, A. V., Vidya, P. J., Shenoy, D. M., Gauns, M., Uskaikar, H., & Aparna, S. G. (2020). Role of oceanic fronts in enhancing phytoplankton biomass in the eastern Arabian Sea during an oligotrophic period. *Marine Environmental Research*, 160, 105023.
50. Kurian, S., Roy, R., Repeta, D. J., Gauns, M., Shenoy, D. M., Suresh, T., ... & Naqvi, S. W. A. (2012). Seasonal occurrence of anoxygenic photosynthesis in Tillari and Selaulim reservoirs, Western India. *Biogeosciences*, 9(7), 2485-2495.
51. Letscher, R. T., Hansell, D. A., Carlson, C. A., Lumpkin, R., & Knapp, A. N. (2013). Dissolved organic nitrogen in the global surface ocean: Distribution and fate. *Global Biogeochemical Cycles*, 27(1), 141-153.
52. Madhupratap, M., Kumar, S. P., Bhattathiri, P. M. A., Kumar, M. D., Raghukumar, S., Nair, K. K. C., & Ramaiah, N. (1996). Mechanism of the biological response to winter cooling in the northeastern Arabian Sea. *Nature*, 384(6609), 549-552.
53. Marra, J., & Barber, R. T. (2005). Primary productivity in the Arabian Sea: A synthesis of JGOFS data. *Progress in Oceanography*, 65(2-4), 159-175.
54. McCreary Jr, J. P., Kohler, K. E., Hood, R. R., & Olson, D. B. (1996). A four-component ecosystem model of biological activity in the Arabian Sea. *Progress in Oceanography*, 37(3-4), 193-240.
55. McCreary Jr, J. P., Kundu, P. K., & Molinari, R. L. (1993). A numerical investigation of dynamics, thermodynamics and mixed-layer processes in the Indian Ocean. *Progress in Oceanography*, 31(3), 181-244.
56. McCreary Jr, J. P., Yu, Z., Hood, R. R., Vinaychandran, P. N., Furue, R., Ishida, A., & Richards, K. J. (2013). Dynamics of the Indian-Ocean oxygen minimum zones. *Progress in Oceanography*, 112, 15-37.
57. McGillicuddy Jr, D. J., & Robinson, A. R. (1997). Eddy-induced nutrient supply and new production in the Sargasso Sea. *Deep Sea Research Part I: Oceanographic Research Papers*, 44(8), 1427-1450.
58. McGillicuddy, D. J., Robinson, A. R., Siegel, D. A., Jannasch, H. W., Johnson, R., Dickey, T. D., ... & Knap, A. H. (1998). Influence of mesoscale eddies on new production in the Sargasso Sea. *Nature*, 394(6690), 263-266.

59. Moffett, J. W., Vedamati, J., Goepfert, T. J., Pratihary, A., Gauns, M., & Naqvi, S. W. A. (2015). Biogeochemistry of iron in the Arabian Sea. *Limnology and Oceanography*, 60(5), 1671-1688.
60. Moore, C. M., Mills, M. M., Arrigo, K. R., Berman-Frank, I., Bopp, L., Boyd, P. W., ... & Ulloa, O. (2013). Processes and patterns of oceanic nutrient limitation. *Nature geoscience*, 6(9), 701-710.
61. Morrison, J. M., Codispoti, L. A., Gaurin, S., Jones, B., Manghnani, V., & Zheng, Z. (1998). Seasonal variation of hydrographic and nutrient fields during the US JGOFS Arabian Sea Process Study. *Deep Sea Research Part II: Topical Studies in Oceanography*, 45(10-11), 2053-2101.
62. Mukherjee, A., Shankar, D., Chatterjee, A., & Vinayachandran, P. N. (2018). Numerical simulation of the observed near-surface East India Coastal Current on the continental slope. *Climate Dynamics*, 50, 3949-3980.
63. Mulet, S., Rio, M. H., Mignot, A., Guinehut, S., & Morrow, R. (2012). A new estimate of the global 3D geostrophic ocean circulation based on satellite data and in-situ measurements. *Deep Sea Research Part II: Topical Studies in Oceanography*, 77, 70-81.
64. Nair, R. R., Ittekkot, V., Manganini, S. J., Ramaswamy, V., Haake, B., Degens, E. T., ... & Honjo, S. (1989). Increased particle flux to the deep ocean related to monsoons. *Nature*, 338(6218), 749-751.
65. Naqvi, S. W. A. (1987). Some aspects of the oxygen-deficient conditions and denitrification in the Arabian Sea. *Journal of Marine research*, 45(4), 1049-1072.
66. Naqvi, S. W. A., Moffett, J. W., Gauns, M. U., Narvekar, P. V., Pratihary, A. K., Naik, H., ... & Ahmed, S. I. (2010). The Arabian Sea as a high-nutrient, low-chlorophyll region during the late Southwest Monsoon. *Biogeosciences*, 7(7), 2091-2100.
67. Parsons, T.R., Maita, Y., & Lalli, C.M. (1984). A manual of chemical and biological methods for seawater analysis. Pergamon, Oxford sized algae and natural seston size fractions. *Marine Ecology Progress Series*. 199, 43-53.
68. Pfannkuche, O., & Lochte, K. (2000). The biogeochemistry of the deep Arabian Sea: overview. *Deep-sea research. Part 2. Topical studies in oceanography*, 47(14), 2615-2628.
69. Pollard, R. T., & Regier, L. (1990). Large variations in potential vorticity at small spatial scales in the upper ocean. *Nature*, 348(6298), 227-229.
70. Prasanna Kumar, S., R. P. Roshin, J. Narvekar, P. K. Dinesh Kumar, and E. Vivekanandan (2009), Response of the Arabian Sea to global warming and associated regional climate shift, *Mar. Environ. Res.*, **68**, 217- 222.
71. Rajagopalan, M. S., Thomas, P. A., Mathew, K. J., Selvaraj, G. D., George, R. M., Mathew, C. V., ... & Antony, G. (1992). Productivity of the Arabian Sea along the southwest coast of India. *CMFRI Bulletin*, 45, 9-37. Habeebrehman et al., 2008,
72. Rejomon, G., DineshKumar, P. K., & Nair, M. (2013). Biogeochemical significance of eddies of the eastern Arabian Sea.

73. Resplandy, L., Lévy, M., Bopp, L., Echevin, V., Pous, S. V. V. S. S., Sarma, V. V. S. S., & Kumar, D. (2012). Controlling factors of the oxygen balance in the Arabian Sea's OMZ. *Biogeosciences*, *9*(12), 5095-5109.
74. Resplandy, L., Lévy, M., Madec, G., Pous, S., Aumont, O., & Kumar, D. (2011). Contribution of mesoscale processes to nutrient budgets in the Arabian Sea. *Journal of Geophysical Research: Oceans*, *116*(C11).
75. Roy, R., Chitari, R., Kulkarni, V., Krishna, M. S., Sarma, V. V. S. S., & Anil, A. C. (2015). CHEMTAX-derived phytoplankton community structure associated with temperature fronts in the northeastern Arabian Sea. *Journal of Marine Systems*, *144*, 81-91.
76. Rudnick, D. L., & Ferrari, R. (1999). Compensation of horizontal temperature and salinity gradients in the ocean mixed layer. *Science*, *283*(5401), 526-529.
77. Rudnick, D. L., & Luyten, J. R. (1996). Intensive surveys of the Azores Front: 1. Tracers and dynamics. *Journal of Geophysical Research: Oceans*, *101*(C1), 923-939.
78. Sabine, C. L., Feely, R. A., Gruber, N., Key, R. M., Lee, K., Bullister, J. L., ... & Rios, A. F. (2004). The oceanic sink for anthropogenic CO₂. *science*, *305*(5682), 367-371.
79. Sarma, V. V. S. S., Delabehra, H. B., Sudharani, P., Remya, R., Patil, J. S., & Desai, D. V. (2015). Variations in the inorganic carbon components in the thermal fronts during winter in the northeastern Arabian Sea. *Marine Chemistry*, *169*, 16-22.
80. Sarma, V. V. S. S., Desai, D. V., Patil, J. S., Khandeparker, L., Aparna, S. G., Shankar, D., ... & Anil, A. C. (2018). Ecosystem response in temperature fronts in the northeastern Arabian Sea. *Progress in Oceanography*, *165*, 317-331.
81. Schoffman, H., Lis, H., Shaked, Y., & Keren, N. (2016). Iron–nutrient interactions within phytoplankton. *Frontiers in plant science*, *7*, 1223.
82. Shafeeque, M., Balchand, A. N., Shah, P., George, G., BR, S., Varghese, E., ... & Platt, T. (2021). Spatio-temporal variability of chlorophyll-a in response to coastal upwelling and mesoscale eddies in the South Eastern Arabian Sea. *International Journal of Remote Sensing*, *42*(13), 4836-4863.
83. Shah, P., Sajeev, R., & Gopika, N. (2015). Study of upwelling along the west coast of India—A climatological approach. *Journal of Coastal Research*, *31*(5), 1151-1158.
84. Shetye, S. R., Gouveia, A. D., Shenoi, S. S. C., Sundar, D., Michael, G. S., Almeida, A. M., & Santanam, K. (1990). Hydrography and circulation off the west coast of India during the southwest monsoon 1987. *Journal of Marine Research*, *48*(2), 359-378.
85. Shetye, S. S., Kurian, S., Gauns, M., & Vidya, P. J. (2019). 2015–16 ENSO contributed reduction in oil sardines along the Kerala coast, south-west India. *Marine Ecology*, *40*(6), e12568.
86. Shetye, S. S., Kurian, S., Vidya, P. J., Gauns, M., Shenoy, D. M., Aparna, S. G., ... & Karapurkar, S. G. (2021). Total organic carbon and its role in oxygen utilization in the eastern Arabian Sea. *Marine Pollution Bulletin*, *163*, 111939.

87. Shetye, S., Pratihary, A., Shenoy, D., Kurian, S., Gauns, M., Naik, H., Nandakumar, K..... & Borker, S. (2023). Rice husk as a potential source of silicate to oceanic phytoplankton. *Science of the Total Environment*, 162941.
88. Smith, S. L., Codispoti, L. A., Morrison, J. M., & Barber, R. T. (1998). The 1994-1996 Arabian Sea Expedition: An integrated, interdisciplinary investigation of the response of the northwestern Indian Ocean to monsoonal forcing. *Deep-sea research. Part II, Topical studies in oceanography*, 45(10-11), 1905-1915.
89. Smitha, B. R., Sanjeevan, V. N., Padmakumar, K. B., Hussain, M. S., Salini, T. C., & Lix, J. K. (2022). Role of mesoscale eddies in the sustenance of high biological productivity in North Eastern Arabian Sea during the winter-spring transition period. *Science of the Total Environment*, 809, 151173.
90. Smitha, B. R., Sanjeevan, V. N., Vimalkumar, K. G., & Revichandran, C. (2008). On the upwelling off the southern tip and along the west coast of India. *Journal of Coastal Research*, (24 (10024)), 95-102.
91. Solanki, H. U., Dwivedi, R. M., Nayak, S. R., Somvanshi, V. S., Gulati, D. K., & Pattnayak, S. K. (2003). Fishery forecast using OCM chlorophyll concentration and AVHRR SST: validation results off Gujarat coast, India. *International Journal of Remote Sensing*, 24(18), 3691-3699.
92. Solanki, H. U., Prakash, P., Dwivedi, R. M., Nayak, S., Kulkarni, A., & Somvamshi, V. S. (2010). Synergistic application of oceanographic variables from multi-satellite sensors for forecasting potential fishing zones: methodology and validation results. *International Journal of Remote Sensing*, 31(3), 775-789.
93. Stone, H. B., Banas, N. S., & MacCready, P. (2018). The effect of alongcoast advection on Pacific Northwest shelf and slope water properties in relation to upwelling variability. *Journal of Geophysical Research: Oceans*, 123(1), 265-286.
94. Stukel, M. R., Song, H., Goericke, R., & Miller, A. J. (2018). The role of subduction and gravitational sinking in particle export, carbon sequestration, and the remineralization length scale in the California Current Ecosystem. *Limnology and Oceanography*, 63(1), 363-383.
95. Subrahmanyam, B., & Robinson, I. S. (2000). Sea surface height variability in the Indian Ocean from TOPEX/POSEIDON altimetry and model simulations. *Marine Geodesy*, 23(3), 167-195.
96. Sweeney, E. N., McGillicuddy Jr, D. J., & Buesseler, K. O. (2003). Biogeochemical impacts due to mesoscale eddy activity in the Sargasso Sea as measured at the Bermuda Atlantic Time-series Study (BATS). *Deep Sea Research Part II: Topical Studies in Oceanography*, 50(22-26), 3017-3039.
97. Trott, C. B., Subrahmanyam, B., & Murty, V. S. N. (2017). Variability of the Somali Current and eddies during the southwest monsoon regimes. *Dynamics of Atmospheres and Oceans*, 79, 43-55.
98. Trott, C. B., Subrahmanyam, B., Chaigneau, A., & Delcroix, T. (2018). Eddy tracking in the northwestern Indian Ocean during southwest monsoon regimes. *Geophysical Research Letters*, 45(13), 6594-6603.

99. Verbrugge, N., Mulet, S., Guinehut, S., & Buongiorno-Nardelli, B. (2017, April). ARMOR3D: A 3D multi-observations T, S, U, V product of the ocean. In *EGU general assembly conference abstracts* (p. 17579).
100. Vipin, P., Sarkar, K., Aparna, S. G., Shankar, D., Sarma, V. V. S. S., Gracias, D. G., ... & Rao, N. S. (2015). Evolution and sub-surface characteristics of a sea-surface temperature filament and front in the northeastern Arabian Sea during November–December 2012. *Journal of Marine Systems*, *150*, 1-11.
101. Wiggert, J. D., Hood, R. R., Banse, K., & Kindle, J. C. (2005). Monsoon-driven biogeochemical processes in the Arabian Sea. *Progress in Oceanography*, *65*(2-4), 176-213.
102. Wiggert, J. D., Murtugudde, R. G., & McClain, C. R. (2002). Processes controlling interannual variations in wintertime (Northeast Monsoon) primary productivity in the central Arabian Sea. *Deep Sea Research Part II: Topical Studies in Oceanography*, *49*(12), 2319-2343.
103. Wyrтки, K., Bennett, E. B., & Rochford, D. J. (1971). *Oceanographic atlas of the international Indian Ocean expedition* (Vol. 531). Washington, DC: National Science Foundation.